IEEE Access
Multidisciplinary | Rapid Review | Open Access Journal

Received 5 July 2022, accepted 15 July 2022, date of publication 25 July 2022, date of current version 28 July 2022.

Digital Object Identifier 10.1109/ACCESS.2022.3193387

RESEARCH ARTICLE

Linear Optimization Based Distribution Grid Flexibility Aggregation Augmented With OLTC Operational Flexibilities

NEELOTPAL MAJUMDAR, MARCEL SARSTEDT, LEONARD KLUß, AND LUTZ HOFMANN
Electric Power Engineering Section, Institute of Electric Power Systems, Leibniz Universität Hannover, 30167 Hanover, Germany

Corresponding author: Neelotpal Majumdar (majumdar@ifes.uni-hannover.de)

This work was supported in part by the Lower Saxony Ministry of Science and Culture through the "Niedersächsisches Vorab" Program under Grant ZN3563, and in part by the Energy Research Centre of Lower Saxony through the Ancillary Services for Reliable Power Grids in Times of Progressive German Energiewende and Digital Transformation [Systemdienstleistungen für sichere Stromnetze in Zeiten fortschreitender Energiewende und digitaler Transformation (SiNED)]-System Services for secure electricity grids in times of advancing energy transition and digital transformation project.

ABSTRACT Ancillary services e.g., voltage control, congestion management and frequency control, require to be compensated increasingly from the Distributed Energy Resources (DERs). DERs are predominantly wind and photo-voltaic power plants, the major share of which are installed at the distribution grid level. Therefore, the previously passive distribution grids require transformation towards a more active role. Provision of ancillary services from the distribution grid level, requires assessment of active and reactive power flexibility (PQ-flexibility) potentials. Furthermore, increased renewable penetration correlates to increased responsibility of the Distribution System Operators (DSOs) for assessing the flexibility potentials. An aggregation of distribution grid potentials, subject to technical grid constraints and technological power limitations, is termed as Feasible Operating Region (FOR) of the distribution grid. The FOR effectively serves as an interface between the DSOs and the Transmission System Operators (TSO), for flexibility exchanges and planning of ancillary services provision. The determination of the FOR is established in current research, using different algorithms e.g stochastic methods, meta-heuristic programming and mathematical optimization techniques. In this paper, an FOR determination algorithm using successive linear programming (sLP) is proposed and validated against established optimization approaches on a uniform medium voltage (MV) grid model. Comparisons reveal competitiveness with established methods and an added advantage of fast calculation times, suitable for real time assessments. Further enhancement of the FOR is proposed, by integrating discrete transformer tap-changing operational flexibilities using a successive mixed integer linear programming (sMILP). Results demonstrate an increase in the flexibility potential from the distribution grid.

INDEX TERMS Ancillary services, flexibility aggregation, feasible operating region, stochastics, meta-heuristics, successive linear programming, mixed-integer linear programming.

I. INTRODUCTION

In future power systems, the reduction of thermal power and carbon footprint requires increased operational planning for ancillary services provision through Distributed Energy Resources (DERs) [1]. Installation of DERs, predominantly at the distribution grid level [2], requires a transition of distribution grids towards a more active role- Active Distribution Networks (ADNs). Ancillary services provision at the transmission level from PQ-flexibilities at the distribution level is undergoing changes according to technical and regulatory specifications [3]–[5]. Estimation of vertical PQ-flexibility potential (between two voltage levels) available for extraction from the lower voltage levels requires an aggregation method. Such an aggregation of potentials essentially serves as an interface between the TSO and DSO for feasibility studies and operational management of the power grid. Aggregation of distribution grid potentials

The associate editor coordinating the review of this manuscript and approving it for publication was Akin Tascikaraoglu.

is subject to technical grid constraints and technological constraints of the generation sources, controllable loads and energy storages. Therefore, it is derived as an area of PQ-flexibility provision, termed as the Feasible Operating Region (FOR). The FOR determination is formulated using different approaches in the present literature, classified into stochastic, metaheuristic and optimization based methods. Stochastic based approaches for determining the flexibility area are presented in [6]. However, suggestions include importance of optimization based methods for reducing computation times and accurate determination of the edges. This is further observed in [7], where the authors optimize a set of stochastic Monte-Carlo simulated scenarios to determine a feasible set. Convex approximation to determine the extremities is suggested. This is demonstrated in [8], where Monte-Carlo based feasibility set determination is then approximated using a convex hull. However, this method does not account for the inaccuracies resulting from regional non-convexities. Studies in [9] expand upon the Monte-Carlo based scenario generation approach for the determination of the FOR, by considering a time-dependency of flexibilities (e.g., time required for operating point adaptation).

In [10], an interior-point based optimization method is presented to circumvent the drawback of determining the extremities. Moreover, the concept of a flexibility cost map is introduced, which considers the maximal cost allocation by network operators for flexibility provision. An angle based sampling strategy is introduced, where the feasible set of boundary points are estimated by a discretized 360° angular scan of the PQ-plane. This strategy is further demonstrated in [11], and an improved strategy based on linear and quadratic cost allocation for the reduction of computation time is presented. The method identifies the FOR using reduced OPF runs. A detailed description of a linear programming based FOR determination approach is presented in [12]. A comparison between the non-linear programming based method in [10] and the linear optimization reveals faster computation time due to linearization. Derivation of linearized power flow sensitivities and an adaptation of the angle-based sampling strategy is used in the aggregation procedure. A follow-up study in [13] investigates the impact of grid topology changes and transformer-tap changing operations on flexibility provision. Permutations and combinations of the discrete switching actions yield multiple FORs with the switching actions as a 3rd dimension. The authors in [14] present a comprehensive comparison of a GAMS based non-linear programming, a quadratically constrained linear program (QCLP) and a particle swarm optimization (PSO) based approach for the determination of the FOR. The criteria for the comparison considers accuracy of edge determination and computation times.

The field of distribution grid flexibility aggregation is evolving to cope with the challenges of renewable integrated future power systems and TSO-DSO cooperation. Recent works present approaches for consideration of stochastic power injections using linearized OPF approaches [15]–[17]. Time-coupling of flexibility provision is presented in [16], [18]. Research in [19] adopts an adapted version of the FOR determination in [12], for a time-based aggregation of flexibilities with grid state estimation. This addresses the reduced observability of distribution grids. Fast computation times indicate usability in real time applications. Application of the FOR from the MV grid level for congestion management at the HV grid level is demonstrated in [20]. A mixed integer linear programming based cost-optimal disaggregation of the FOR based flexibility provision addresses the flexibility market characteristics [21].

Even though [12] validates the linear optimization method based FOR determination, the comparability with recent developments is deemed important. Adaptation to the linear optimization method is required to ensure comparable results. Furthermore, although [13] considers transformer flexibilities, independent OPF runs to determine a discrete 3-dimensional FOR for each tap-changer settings is proposed. Since, such a three dimensional aspect is difficult for integration in power system operational management, corresponding adaptations are required. Therefore, in this paper, novel sampling strategies for linear optimization based FOR determination are presented, that strive to ensure comparability of result quality with established optimization methods presented in [14]. Simultaneously, fast computation times are ensured. Advantages include application in real time-based aggregations and assessment of a multitude of uncertain scenarios. The FOR is further adapted considering linearized transformer sensitivities, for a 2-dimensional enhancement of the flexibility area provision. According to the authors' knowledge, such an application of discrete transformer tap-sensitivities in the FOR context is not mentioned in existing literature.

The paper is divided into the following sub-parts: section II presents the mathematical background for deriving the linear sensitivities; section III presents the methodology for the determination of the FOR; section IV describes the investigated grid topology; in section V the results are presented along with corresponding analyses; section VI concludes the topic with suggestions regarding further work in the research.

II. METHODOLOGY FOR DETERMINATION OF THE FEASIBLE OPERATING REGION

The determination of the FOR of the underlying voltage level is formulated as an optimal powerflow problem. The power flow (up-/ down-regulation of injected power at the nodes), is incrementally adapted in successive samples (or steps). Correspondingly, the maximum potential provision of active and reactive power exchange at the MV-HV interconnection is determined for each sampled adjustment. The interconnection power flow (IPF) is subject to technical grid constraints and technology constraints of the PQ-flexibilities. Successive linear programming (sLP) method, which is widely used in OPF formulations [22]–[24], is selected for solving the problem formulation.

The non-linear power flow equations are linearized around the point of operation, around which validity is ensured. The algorithm is solved iteratively, using the optimization results at each iteration step for a power flow calculation to obtain the adapted grid state. Therefore, an iterative adaptation of the operating points of the flexibilities, maximum and minimum range of the PQ-flexibilities and technical constraints for each iteration, is required. These adaptations serve as the input for the subsequent iteration. A convergence criterion satisfying a permissible tolerance band stops the iterative process, yielding the results of the algorithm for each sample.

A. LINEARIZED POWER FLOW EQUATIONS

The notations for the presented equations throughout the paper are described:

- The variables are specified with appropriate indices or as vectors
- In vector notation, matrices are symbolised in bold and in capital letters (e.g., $\boldsymbol{A}$). One-dimensional vectors are specified with small and bold letters (e.g., $\boldsymbol{a}$), single-valued scalars are indicated by capital or small letters (e.g., A or a).

The power flow equations are presented in polar coordinates as follows:

$$P_i = V_i^2 Y_{ii} \cos\theta_{ii} + \sum_{\substack{j=1 \\ i\neq j}}^{n} V_i V_j Y_{ij} \cos(\delta_i - \delta_j - \theta_{ij}) \quad (1)$$

$$Q_i = -V_i^2 Y_{ii} \sin\theta_{ii} + \sum_{\substack{j=1 \\ i\neq j}}^{n} V_i V_j Y_{ij} \sin(\delta_i - \delta_j - \theta_{ij}) \quad (2)$$

The indices $i, j \in n$ represent the bus numbers, where n specifies the total number of busses in the system. Linearization of the power flow equations with Taylor's first order approximation yields sensitivities in the form of the Jacobian matrix. Inverting the Jacobian matrix ($\boldsymbol{J}^{-1}$) results in the desired angle-power ($\delta - p, \delta - q$), and voltage-power ($v - p, v - q$) sensitivities[1].

$$\begin{bmatrix} \Delta\boldsymbol{\delta} \\ \Delta\boldsymbol{v} \end{bmatrix} = \boldsymbol{J}^{-1} \begin{bmatrix} \Delta\boldsymbol{p} \\ \Delta\boldsymbol{q} \end{bmatrix} \quad (3)$$

with

$$\boldsymbol{J}^{-1} = \begin{bmatrix} \frac{\partial\boldsymbol{\delta}}{\partial\boldsymbol{p}} & \frac{\partial\boldsymbol{\delta}}{\partial\boldsymbol{q}} \\ \frac{\partial\boldsymbol{v}}{\partial\boldsymbol{p}} & \frac{\partial\boldsymbol{v}}{\partial\boldsymbol{q}} \end{bmatrix}$$

[1]Voltage dependencies of loads is neglected (constant loads are considered). Inclusion of voltage dependencies requires a voltage dependent adaptaion of the shunt impedances in equations (1) and (2). This influences the sensitivities for a further accurate estimation of the grid conditions. However, in the scope of this work, this augmentation is not deemed significant

The sensitivities are further expanded upon by deriving sensitivities with regards to transformer tap-changing operation, thus, integrating OLTC operation as an additional flexibility. The corresponding branch power flow equations, with discrete tap-changing variables (τ) are presented as follows [24]:

$$P_{i,t} = V_i^2 Y_{ii} \cos\theta_{ii} + V_i V_j \frac{Y_{ij}}{\tau} \cos(\delta_i - \delta_j - \theta_{ij}) \quad (4)$$

$$P_{j,t} = V_j^2 \frac{Y_{jj}}{\tau^2} \cos\theta_{jj} + V_i V_j \frac{Y_{ij}}{\tau} \cos(\delta_j - \delta_i - \theta_{ij}) \quad (5)$$

$$Q_{i,t} = -V_i^2 Y_{ii} \sin\theta_{ii} + V_i V_j \frac{Y_{ij}}{\tau} \sin(\delta_i - \delta_j - \theta_{ij}) \quad (6)$$

$$Q_{j,t} = -V_j^2 \frac{Y_{jj}}{\tau^2} \sin\theta_{jj} + V_i V_j \frac{Y_{ij}}{\tau} \sin(\delta_j - \delta_i - \theta_{ij}) \quad (7)$$

with

$$\tau = (1 + \sigma \frac{\Delta\eta}{100}); \sigma \in \mathbb{Z} \mid -10 \leq \sigma \leq 10$$

s.t for

$$\Delta\eta = 0.25; \tau \in [0.975, 1.025]$$

for $i \in n$, and $i, t \in n_t$, where n_t represents the set of receiving and sending end buses connected with a transformer. σ represents the discrete-tap settings within the integer set of numbers $\mathbb{Z}$. The range of σ and the specification of $\Delta\eta$ can further be validated from [25], [26]. The influence of the tap-changing operation at the MV-HV interconnection branch, therefore, affects the power flow, and correspondingly can influence the FOR. Consequently, the active and reactive power branch flow sensitivities with regards to the discrete tap-setting variable are derived:

$$\frac{\partial P_{i,t}}{\partial\sigma}; \frac{\partial P_{j,t}}{\partial\sigma}; \frac{\partial Q_{i,t}}{\partial\sigma}; \frac{\partial Q_{j,t}}{\partial\sigma} \quad (8)$$

This work neglects the phase sensitivities of the transformer taps, as their usage is limited in the present scenario (phase-shifting transformers are not applied in practice at the MV-HV interconnections). Correspondingly, the angle and voltage sensitivities for all buses are enhanced by combining (3) and (8), resulting in angle-tap ($\delta - \sigma$) and voltage-tap ($v - \sigma$) sensitivities:

$$\frac{\partial\delta_i}{\partial\sigma} = \frac{\partial\delta_i}{\partial P_{i,t}}\frac{\partial P_{i,t}}{\partial\sigma} + \frac{\partial\delta_i}{\partial P_{j,t}}\frac{\partial P_{j,t}}{\partial\sigma} + \frac{\partial\delta_i}{\partial Q_{i,t}}\frac{\partial Q_{i,t}}{\partial\sigma} + \frac{\partial\delta_i}{\partial Q_{j,t}}\frac{\partial Q_{j,t}}{\partial\sigma} \quad (9)$$

$$\frac{\partial v_i}{\partial\sigma} = \frac{\partial v_i}{\partial P_{i,t}}\frac{\partial P_{i,t}}{\partial\sigma} + \frac{\partial v_i}{\partial P_{j,t}}\frac{\partial P_{j,t}}{\partial\sigma} + \frac{\partial v_i}{\partial Q_{i,t}}\frac{\partial Q_{i,t}}{\partial\sigma} + \frac{\partial v_i}{\partial Q_{j,t}}\frac{\partial Q_{j,t}}{\partial\sigma} \quad (10)$$

Subsequently, the bus voltage magnitude and angle deviations are expressed as follows:

$$\Delta\boldsymbol{\delta} = \frac{\partial\boldsymbol{\delta}}{\partial\boldsymbol{p}}\Delta\boldsymbol{p} + \frac{\partial\boldsymbol{\delta}}{\partial\boldsymbol{q}}\Delta\boldsymbol{q} + \frac{\partial\boldsymbol{\delta}}{\partial\boldsymbol{\sigma}}\Delta\boldsymbol{\sigma} \quad (11)$$

$$\Delta\boldsymbol{v} = \frac{\partial\boldsymbol{v}}{\partial\boldsymbol{p}}\Delta\boldsymbol{p} + \frac{\partial\boldsymbol{v}}{\partial\boldsymbol{q}}\Delta\boldsymbol{q} + \frac{\partial\boldsymbol{v}}{\partial\boldsymbol{\sigma}}\Delta\boldsymbol{\sigma} \quad (12)$$

Within an optimization environment, the deviations are bound within constraints subject to technical network limitation, as previously discussed. The method is further extended to include branch current constraints, the formulation for which is adapted from a well established work on branch current sensitivities [27], [28]. The formulation is described as:

$$\Delta \boldsymbol{i} = \boldsymbol{ID}_{\mathrm{TT}} \Delta \boldsymbol{\delta}_{\mathrm{T}} + \boldsymbol{IU}_{\mathrm{TT}} \Delta \boldsymbol{v}_{\mathrm{T}} \tag{13}$$

with

$$\boldsymbol{ID}_{\mathrm{TT}} = \frac{\partial \Delta \boldsymbol{i}_{\mathrm{T}}}{\partial \boldsymbol{\delta}_{\mathrm{T}}}; \boldsymbol{IU}_{\mathrm{TT}} = \frac{\partial \Delta \boldsymbol{i}_{\mathrm{T}}}{\partial \boldsymbol{v}_{\mathrm{T}}}$$

The subscript T refers to the branch terminals (T $= 2l$, where l represents the number of lines or branches). The subscript TT describes current sensitivities for a corresponding deviation of the terminal bus voltage angles and magnitudes (terminal sensitivities). However, in the presented optimization environment, the variables used are bus voltage magnitudes and angles. Therefore, the terminal sensitivity matrix is multiplied with the nodal-incidence matrix, to yield terminal-bus sensitivity matrices $\boldsymbol{ID}_{\mathrm{TB}}$ and $\boldsymbol{IU}_{\mathrm{TB}}$.

It is imperative to mention the usage of transformer sensitivities to influence the branch power flow (8), in addition to the angle-tap and voltage-tap sensitivities. However, negligence of the phase-shifting property, as previously mentioned, effectively influences a dominant sensitivity of the tap-changing operation on the reactive power flow. The corresponding influence on the active power flow is negligible. Therefore, the reactive power transfer sensitivity from (8) is used for integration into the optimization environment.

III. DETERMINATION OF THE FEASIBLE OPERATING REGION

A. FORMULATION OF THE SUCCESSIVE LINEAR OPTIMIZATION METHODOLOGY

The linear optimal power flow environment is formulated as:

$$\begin{aligned} &\min \boldsymbol{c}^{\mathrm{T}} \boldsymbol{x} \mid \boldsymbol{x} = [\Delta \boldsymbol{p}^{\mathrm{T}}, \Delta \boldsymbol{q}^{\mathrm{T}}, \Delta \boldsymbol{\sigma}^{\mathrm{T}}, \Delta \boldsymbol{\delta}^{\mathrm{T}}, \Delta \boldsymbol{v}^{\mathrm{T}}]^{\mathrm{T}}_{m,1}; \\ &\quad \boldsymbol{c} = [c_k]^{\mathrm{T}}_{m,1}, k \in [1, m] \cap \mathbb{Z}; m = 4n + 1 \\ &\quad \boldsymbol{A}_{\mathrm{ineq}} \boldsymbol{x} \leq \boldsymbol{b}_{\mathrm{ineq}}; \boldsymbol{A}_{\mathrm{eq}} \boldsymbol{x} = \boldsymbol{b}_{\mathrm{eq}} \\ &\text{s.t } \Delta \boldsymbol{p}_{\min} \leq \Delta \boldsymbol{p} \leq \Delta \boldsymbol{p}_{\max} \\ &\quad \Delta \boldsymbol{q}_{\min} \leq \Delta \boldsymbol{q} \leq \Delta \boldsymbol{q}_{\max} \\ &\quad \Delta \boldsymbol{\sigma}_{\min} \leq \Delta \boldsymbol{\sigma} \leq \Delta \boldsymbol{\sigma}_{\max} \end{aligned} \tag{14}$$

$\boldsymbol{c}$ refers to the vector of costs c_k (penalty factors) associated with the variable vector $\boldsymbol{x}$. The inequality (subscript 'ineq') and equality (subscript 'eq') matrices divided into the upper bound (subscript 'ub') and lower bound (subscript 'lb') matrices are expressed as:

$$\begin{aligned} \boldsymbol{A}_{\mathrm{ineq}} &= \begin{bmatrix} \boldsymbol{A}_{\mathrm{ineq,ub}} \\ \boldsymbol{A}_{\mathrm{ineq,lb}} \end{bmatrix}; \boldsymbol{b}_{\mathrm{ineq}} = \begin{bmatrix} \boldsymbol{b}_{\mathrm{ineq,ub}} \\ \boldsymbol{b}_{\mathrm{ineq,lb}} \end{bmatrix} \\ \boldsymbol{A}_{\mathrm{eq}} &= \begin{bmatrix} \boldsymbol{A}_{\mathrm{eq,ub}} \\ \boldsymbol{A}_{\mathrm{eq,lb}} \end{bmatrix}; \boldsymbol{b}_{\mathrm{eq}} = \begin{bmatrix} \boldsymbol{b}_{\mathrm{eq,ub}} \\ \boldsymbol{b}_{\mathrm{eq,lb}} \end{bmatrix} \\ \boldsymbol{A}_{\mathrm{ineq,lb}} &= -\boldsymbol{A}_{\mathrm{ineq,ub}}; \boldsymbol{A}_{\mathrm{eq,lb}} = -\boldsymbol{A}_{\mathrm{eq,ub}} \\ \boldsymbol{b}_{\mathrm{ineq,lb}} &= -\boldsymbol{b}_{\mathrm{ineq,ub}}; \boldsymbol{b}_{\mathrm{eq,lb}} = -\boldsymbol{b}_{\mathrm{eq,ub}} \end{aligned}$$

The upper bound matrices specify adherence to the maximal grid constraints, whereas, the lower bound matrices correspond to the minimal grid constraints. The matrices are specified as follows:

$$\boldsymbol{A}_{\mathrm{ineq,ub}} = \begin{bmatrix} \frac{\partial \boldsymbol{\delta}}{\partial \boldsymbol{p}} & \frac{\partial \boldsymbol{\delta}}{\partial \boldsymbol{q}} & \frac{\partial \boldsymbol{\delta}}{\partial \boldsymbol{\sigma}} & \boldsymbol{0}_{n,n} & \boldsymbol{0}_{n,n} \\ \frac{\partial \boldsymbol{v}}{\partial \boldsymbol{p}} & \frac{\partial \boldsymbol{v}}{\partial \boldsymbol{q}} & \frac{\partial \boldsymbol{v}}{\partial \boldsymbol{\sigma}} & \boldsymbol{0}_{n,n} & \boldsymbol{0}_{n,n} \\ \boldsymbol{0}_{1,n} & \boldsymbol{0}_{1,n} & 0 & \boldsymbol{ID}_{\mathrm{TB}} & \boldsymbol{IU}_{\mathrm{TB}} \end{bmatrix}_{3n,m}$$

$$\boldsymbol{A}_{\mathrm{eq,ub}} = \begin{bmatrix} \frac{\partial \boldsymbol{\delta}}{\partial \boldsymbol{p}} & \frac{\partial \boldsymbol{\delta}}{\partial \boldsymbol{q}} & \frac{\partial \boldsymbol{\delta}}{\partial \boldsymbol{\sigma}} & -\boldsymbol{1}_{n,n} & \boldsymbol{0}_{n,n} \\ \frac{\partial \boldsymbol{v}}{\partial \boldsymbol{p}} & \frac{\partial \boldsymbol{v}}{\partial \boldsymbol{q}} & \frac{\partial \boldsymbol{v}}{\partial \boldsymbol{\sigma}} & \boldsymbol{0}_{n,n} & -\boldsymbol{1}_{n,n} \\ \boldsymbol{0}_{1,n} & \boldsymbol{0}_{1,n} & 0 & \boldsymbol{0}_{1,n} & \boldsymbol{0}_{1,n} \end{bmatrix}_{3n,m}$$

$$\boldsymbol{b}_{\mathrm{ineq,ub}} = \begin{bmatrix} \boldsymbol{\delta}_{\max} - \boldsymbol{\delta}_0 \\ \boldsymbol{v}_{\max} - \boldsymbol{v}_0 \\ \boldsymbol{i}_{\max} - \boldsymbol{i}_0 \\ \hline \boldsymbol{i}_0 \end{bmatrix}_{3n,1}; \quad \boldsymbol{b}_{\mathrm{eq,ub}} = \begin{bmatrix} \boldsymbol{0}_{n,1} \\ \boldsymbol{0}_{n,1} \\ \boldsymbol{0}_{n,1} \end{bmatrix}_{3n,1}$$

Dimension $m = 4n + 1$, refers to the 4 vectors ($\Delta \boldsymbol{p}, \Delta \boldsymbol{q}, \Delta \boldsymbol{\delta}, \Delta \boldsymbol{v} \in \boldsymbol{x}$) and the scalar transformer variable ($\Delta \sigma$), since, the transformer sensitivity is a single variable, considered only for the MV-HV interconnection bus. The subscript 'max','min' and '0' correspondingly refer to the maximum, minimum constraint limits and the current operating point.

B. INTRODUCTION OF SLACK VARIABLES

Slack variables are effectively applied in OPF algorithms for diagnostics and addition of soft constraints [22], [23]. In this work, the OPF formulation is enhanced by including two types of slack variables, distinguished by the nature of their respective cost terms. Depending on the objective, the cost terms are manipulated to penalise or reward the slack variables. The rows pertaining to the constraints for angle, voltage and current variables ($\Delta \boldsymbol{\delta}, \Delta \boldsymbol{v}, \Delta \boldsymbol{i}$) are augmented with slack variables ($\tilde{\boldsymbol{x}}_{\mathrm{slack}}$) associated with penalty cost factors. These determine the causes of possible infeasibilities. For example, reactive power dispatch being a localized problem, requires mitigation of localized voltage violations via proximal flexibility provision. Therefore, unavailability of sufficient flexibility at proximal nodes leads to infeasibility of the solution. Slack variables enable the solution to converge, while determining the specific nodes, where flexibility provision is required. The penalty costs are allocated sufficiently high terms to restrict the usage of slack variables only in cases of infeasibility and prevent inadvertent abuse.

$$\begin{aligned} &\boldsymbol{A}_{\mathrm{ineq,ub}} \boldsymbol{x} - \boldsymbol{A}_{\mathrm{slack}} \tilde{\boldsymbol{x}}_{\mathrm{slack}} \leq \boldsymbol{b}_{\mathrm{ub}} \\ &\boldsymbol{A}_{\mathrm{ineq,lb}} \boldsymbol{x} + \boldsymbol{A}_{\mathrm{slack}} \tilde{\boldsymbol{x}}_{\mathrm{slack}} \leq \boldsymbol{b}_{\mathrm{lb}} \\ &\boldsymbol{A}_{\mathrm{slack}} = \mathrm{diag}(1) = \begin{bmatrix} 1 & & & \\ & 1 & & \\ & & \ddots & \\ & & & 1 \end{bmatrix} \end{aligned} \tag{15}$$

Furthermore, as mentioned above, slack variables are also introduced to reward the objective. In the scope of this work, the determination of maximal provision of active and reactive vertical power exchanges at the MV-HV interconnection is of importance. Therefore, slack variables are introduced for fulfillment of these criteria for every sampled adaptation of the vertical power flow.

$$\begin{aligned}\sum_{d=1}^{n}\Delta P_d - 1\cdot x_{\text{slack,p}} = 0 \mid \sum_{d=1}^{n}\Delta P_d = \tilde{P}_{\text{vert}}\\ \sum_{d=1}^{n}\Delta Q_d - 1\cdot x_{\text{slack,q}} = 0 \mid \sum_{d=1}^{n}\Delta Q_d = \tilde{Q}_{\text{vert}}\end{aligned} \tag{16}$$

where $d \in n$ indicates the buses equipped with decentral sources for the investigated scenario, and subscript 'vert' represents the vertical power exchange (IPF). The subscripts 'p' and 'q' specify the respective slack variables for the active and reactive power exchange. The cost factors associated with the slack variables are negative for maximum positive Q_{vert} provision and positive for maximum negative Q_{vert} provision, thus, enabling maximal utilization of respective positive/negative reactive power injection from the individual devices. For P_{vert} provision, negative cost allows maximum possible increase of active power demand at the nodes (down-regulation is considered for the DERs). However, analogous implementation of up-regulation is possible by allocation of positive cost terms for $x_{\text{slack,p}}$.

The linear optimal power flow formulation is accordingly augmented as follows:

$$\begin{aligned}\min\ & \boldsymbol{c}^{\text{T}}\boldsymbol{x} \mid \boldsymbol{x} = [\Delta\boldsymbol{p}^{\text{T}}, \Delta\boldsymbol{q}^{\text{T}}, \Delta\boldsymbol{\sigma}^{\text{T}}, \Delta\boldsymbol{\delta}^{\text{T}}, \Delta\boldsymbol{v}^{\text{T}}, \boldsymbol{x}_{\text{slack}}^{\text{T}}]_{m,1}^{\text{T}};\\ & \boldsymbol{c} = [c_k]_{m,1}^{\text{T}}, k = [1, m] \cap \mathbb{Z}; m = 4n+1\\ & \tilde{\boldsymbol{A}}_{\text{ineq}}\boldsymbol{x} \le \tilde{\boldsymbol{b}}_{\text{ineq}}; \tilde{\boldsymbol{A}}_{\text{eq}}\boldsymbol{x} = \tilde{\boldsymbol{b}}_{\text{eq}}\\ \text{s.t}\ & \Delta\boldsymbol{p}_{\min} \le \Delta\boldsymbol{p} \le \Delta\boldsymbol{p}_{\max}\\ & \Delta\boldsymbol{q}_{\min} \le \Delta\boldsymbol{q} \le \Delta\boldsymbol{q}_{\max}\\ & \Delta\boldsymbol{\sigma}_{\min} \le \Delta\boldsymbol{\sigma} \le \Delta\boldsymbol{\sigma}_{\max}\\ & \boldsymbol{x}_{\text{slack,min}} \le \boldsymbol{x}_{\text{slack}} \le \boldsymbol{x}_{\text{slack,max}}\end{aligned} \tag{17}$$

with

$$\boldsymbol{x}_{\text{slack}} = \begin{bmatrix}\tilde{\boldsymbol{x}}_{\text{slack}}\\ x_{\text{slack,p}}\\ x_{\text{slack,q}}\end{bmatrix}; \tilde{\boldsymbol{A}}_{\text{ineq,ub}} = \left[\begin{array}{c|c}\boldsymbol{A}_{\text{ineq,ub}} & \\ \boldsymbol{A}_{\text{vert,p}} & \boldsymbol{A}_{\text{slack}}\\ \boldsymbol{A}_{\text{vert,q}} & \end{array}\right];$$

$$\tilde{\boldsymbol{b}}_{\text{ineq,ub}} = \begin{bmatrix}\boldsymbol{b}_{\text{ineq,ub}}\\ 0\\ 0\end{bmatrix}$$

where

$$\begin{bmatrix}\boldsymbol{A}_{\text{vert,p}}\\ \boldsymbol{A}_{\text{vert,q}}\end{bmatrix} = \begin{bmatrix}\mathbf{1}_{1,\text{n}} & \mathbf{0}_{1,\text{n}} & 0 & \mathbf{0}_{1,\text{n}} & \mathbf{0}_{1,\text{n}}\\ \mathbf{0}_{1,\text{n}} & \mathbf{1}_{1,\text{n}} & \dfrac{\partial Q_{j,\tau}}{\partial\sigma} & \mathbf{0}_{1,\text{n}} & \mathbf{0}_{1,\text{n}}\end{bmatrix}$$

The transformer branch reactive power flow sensitivity is included for influencing the branch reactive power flow utilization. The equality matrices formulation is augmented accordingly.

C. SAMPLED AGGREGATION OF DISTRIBUTION GRID POTENTIALS (FOR DETERMINATION)

The OPF algorithm is solved for sampled adaptation of the power flow. For successive incremental reductions of active power injection from the DER technologies, the maximum positive and negative reactive power provision is determined. Therefore, the generalized OPF formulation for distribution grid flexibility aggregation is described as:

$$\begin{aligned}&\max \pm \Delta Q_{\text{vert},k}\\ &\text{s.t}\ \Delta\tilde{P}_{\text{vert},k} = \sum_{d=1}^{n}\Delta P_d\\ &\qquad \Delta\tilde{Q}_{\text{vert},k} = \sum_{d=1}^{n}\Delta Q_d\\ &\qquad \Delta P_{d,\min} \le \Delta P_{d,\text{max}} \le \Delta P_{d,\max}\\ &\qquad \Delta Q_{d,\min} \le \Delta Q_{d,\text{max}} \le \Delta Q_{d,\max}\\ &\qquad \boldsymbol{v}_{\min} \le \boldsymbol{v}_0 + \Delta\boldsymbol{v} \le \boldsymbol{v}_{\max}\\ &\qquad \boldsymbol{i}_{\min} \le \boldsymbol{i}_0 + \Delta\boldsymbol{i} \le \boldsymbol{i}_{\max}\end{aligned} \tag{18}$$

Since, the MV-HV interconnection branch connects the MV grid with the HV node (considered as slack), maximization of the vertical exchanges are maximized through utilization of individual devices, see (16). The symbols $\tilde{P}_{\text{vert}}$ and $\tilde{Q}_{\text{vert}}$ differentiate from P_{vert} and Q_{vert}, obtained from determining the interconnection power transfer from power flow calculations, using the corresponding optimal solution. A sampled adaption enables the analysis of varied potential of Q_{vert} provision, subject to the influence of the active power flow in the grid. The effect is of importance due to the high $\frac{R}{X}$ ratio of the MV grid level. A successive reduction of power injection from the decentralized sources, for example, requires increased power flow from the HV grid level. Therefore, receiving end nodes are subject to an increased voltage drop, correspondingly affecting the Q_{vert} provision of the MV grid. This is attributed to a reduced security margin from the absolute voltage limits, due to deviations in operational bus voltages.

Figure 1 illustrates an exemplary FOR with the number of samples $k = 10$. The segmentation with increasing transparency corresponds to increasing active power flow on the x-axis. The dotted markings represent the maximal and minimal reactive power provision determined for each step-wise increment in active power flow. A decrease in reactive power provision is observed with successively segmented power flows, attributed to the reduced security margin of the voltage band.

The sampled aggregation method is described in Figure 2. Figure 3 presents the schematic representations of different state of the art sampling strategies. A detailed discussion is provided in [14]. The angle-based sampling strategy that samples the FOR margin at different angle samples, is unsuitable for integration in a linearized optimization context. This is attributed to the increased deviations between the boundary points and the initial start point. However,

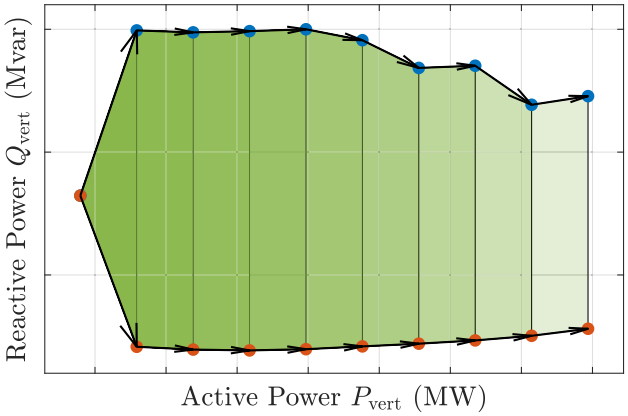

FIGURE 1. Illustration of a sampled FOR with no. of samples (k)=10.

the validity of linearized sensitivities is accurate around the initial point of operation. This limitation can be circumvented by using an iterative process, using the optimal solution in power flow calculations, and correspondingly adapting them, to ensure validity.

The set-point based sampling strategy is adapted for a linear optimization context. Starting from an initial point, the samples are determined successively, such that each successive active power set point of the devices is used as a starting point for the next optimization step. The deviation between successive active power samples is reduced, increasing accuracy of the linear sensitivities. The optimization results are used in power flow calculations and iterated to ensure feasibility considering applied constraints.

The set-point based iterative sampling strategy is an enhancement on the set-point based strategy by iterating upon the boundary points of the FOR. Iterations are used to ensure a maximal possible utilization of the flexibilities, and reduce deviations between optimization results and power flow calculations. Therefore, an accurate approximation for ensuring congruency of the results is an additional enhancement, discussed in results (section V). The number of iterations are selected empirically to achieve sufficient accuracy.

The Q_{vert} deviation reduced strategy, further reduces the deviations between successive samples by using the margin points as the initial operating points for each successive optimization step. Due to minimal deviations between the successive points, increased accuracy of the linear sensitivities is achieved. Therefore, a reduction in computation time, is attributed to decreased iterations for validating the optimal solution against power flow calculations.

D. COMPARISON WITH ESTABLISHED OPF BASED FOR DETERMINATION METHODS

The linear optimization based FOR determination is further validated against previously established methods. The methods, namely, a GAMS based non-linear programming (NLP), a Particle Swarm Optimization (PSO) and a quadratically constrained linear programming (QCLP) algorithm,

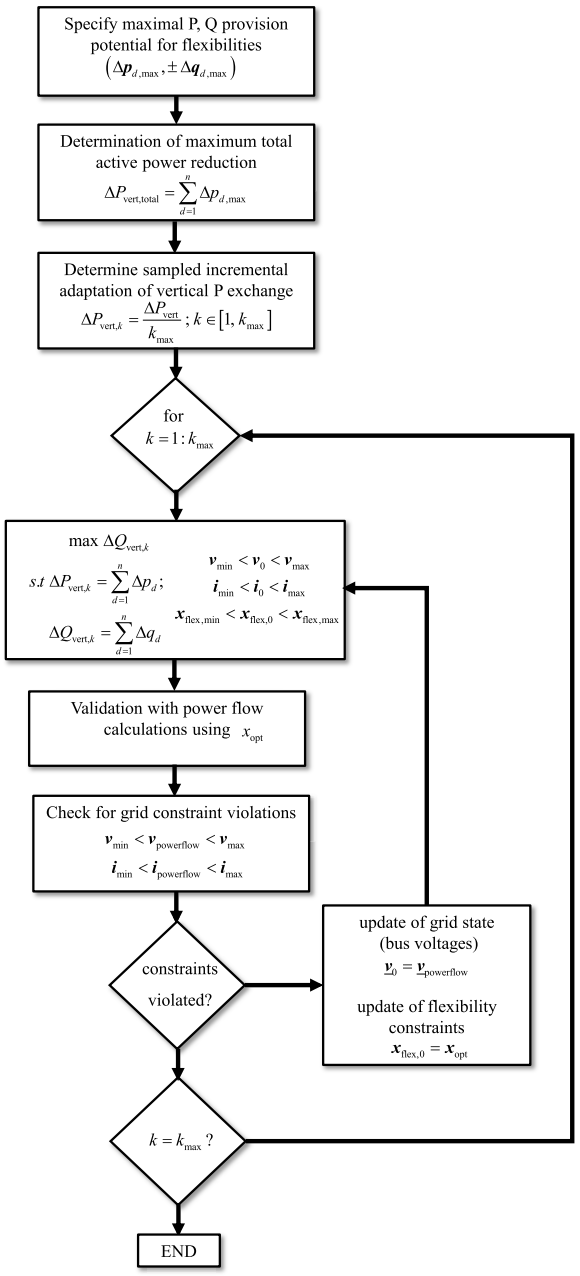

FIGURE 2. Algorithmic description of a generalized FOR determination using linearized optimization methods.

are explained in detail [14]. An area comparison reveals comparability and practicability of linear programming for an FOR based PQ-flexibility aggregation. A comparison of computation times establishes its suitability for usage in fast calculation scenarios, e.g., real time flexibility assessment and impact of renewable power uncertainties.

E. TECHNICAL CONSIDERATIONS AND ASSUMPTIONS

The technical PQ-capabilities of the converter connected DERs are described with different shapes subject to grid codes and regulations of corresponding network operators. Figure 4 presents some common PQ-capability curves that are

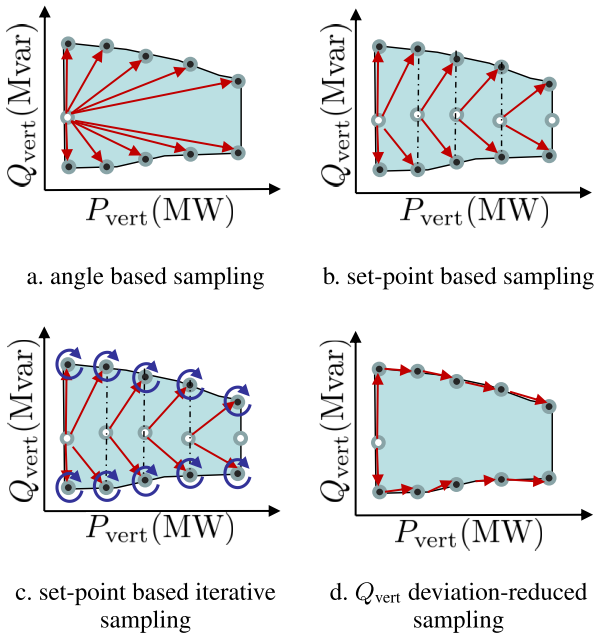

FIGURE 3. Sampling strategies used in determination of the FOR.

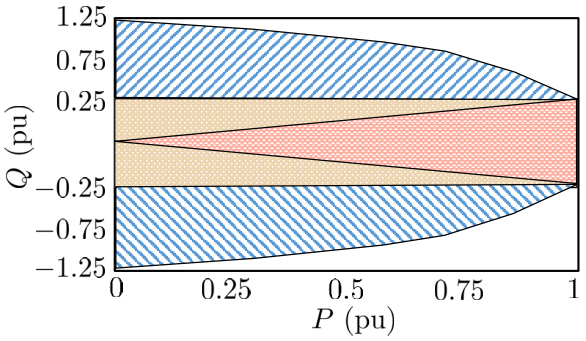

FIGURE 4. PQ-capabilities for converter connected wind and solar DER technologies (D-shaped, rectangular shaped, triangular shaped).

considered in technical implementations [29]. A d-shaped, rectangular or triangular PQ-capability is usually prescribed, subject respectively to device capabilities, constant reactive power output or a constant power factor provision. Further complex modifications can be prescribed by the corresponding network operator as demonstrated in Figure 5. In the scope of this work, a rectangular shaped PQ-capability (a clipped version of the Variant IV)) is considered for ease of implementation in linear optimization. A triangular PQ-capability can be, however, analogously implemented owing to the linear characteristic. However, a more complex non-linear shape, e.g the 'd-shaped' arrangement requires simplification in the form of a piecewise linearization formulation (e.g. Variant VI).

The determination of the FOR at the MV-HV interconnection for a radial distribution grid is illustrated in Figure 6. The PQ-capabilities of the DER technologies at the MV/LV grid level are represented as standard, simplified PQ-polygons. These are subsequently aggregated to determine the potential

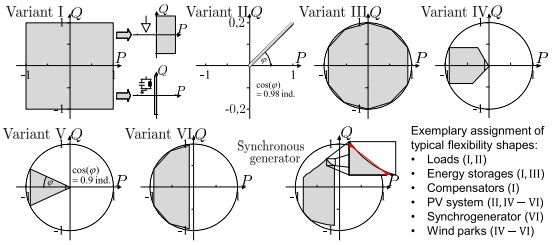

FIGURE 5. Typical PQ-capability curves of different technologies.

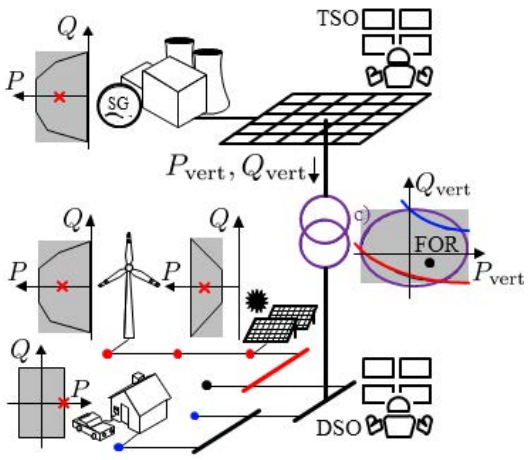

FIGURE 6. A schematic representation of FOR determination for a radial distribution grid.

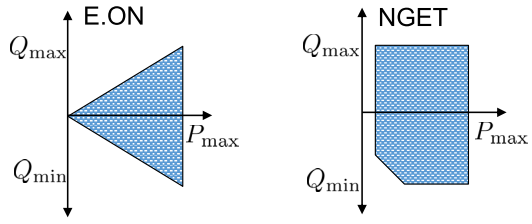

FIGURE 7. Exemplary PQ-capabilities as prescribed by E.ON (Germany) and N.GET (U.K).

FOR at the MV-HV interconnection. The resulting shape is non-linear and possibly non-convex, subject to grid and technology constraints and grid losses due to power transfer.

Exemplary standard PQ-capabilities specified by different network operators like E.ON (Germany) and N.GET (U.K) are described in Figure 7 [29].

Assumptions and further technical considerations implemented in the scope of this work are detailed as follows:

- The device reactive power capabilities are constrained between $q_{d,\min} = -p_{d,\max} \tan\phi$ and $q_{d,\max} = p_{d,\max} \tan\phi$, with $\cos\phi \in [0.85, 0.9]$
- Active power flexibilities are subject to down-regulation ($0 \leq p_d \leq p_{d,\max}$), as DERs are assumed to be operating at the MPPT mode.

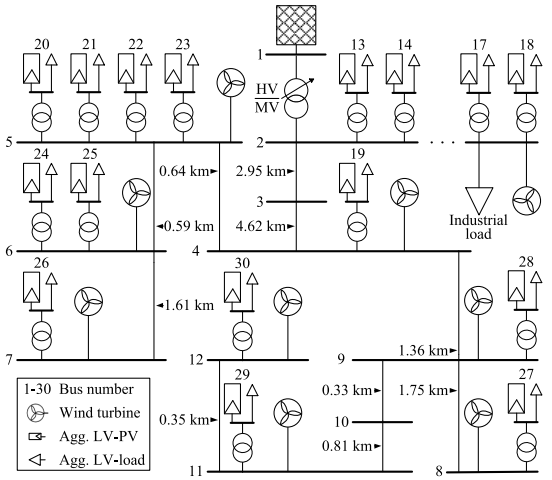

FIGURE 8. Adapted Cigre MV/LV grid topology.

- A detailed specification of line, transformer and load parameters is presented in [14].
- Bus voltages are constrained within a range of ±10% of the nominal voltage (0.9 pu $\leq v \leq$ 1.1 pu)
- Cost for operating individual devices (active and reactive power regulation) are not considered, as economic aspects are not focused in the undertaken study. However, for monotonically increasing behaviour of active power (down-regulation), linear cost terms can be considered. Reactive power which exhibits non-monotonicity requires linear cost terms in conjunction with absolute cost formulation [30].

F. TOOLBOX FOR THE OPTIMIZATION ENVIRONMENT

The successive linear programming formulation (sLP) is achieved using robust interior-point methods of the LINPROG method, and integrations of integer variables for the OLTC tap-set flexibilities is performed using the 'branch and bound' algorithm of the INTLINPROG method [31]. Computations are performed on a computer with a 1.6 GHz. i5-8365U processor and 16 GB RAM.

IV. THE INVESTIGATED NETWORK TOPOLOGY

Investigations are performed on an adapted Cigre MV grid model, integrated with a power flow dataset representing corresponding renewable penetration and load profile for the examined time frame [32]. The radial nature of the grid is typical in Europe, and establishes comparability with studies conducted in this area [12], [14].

The power system comprises of 3 different voltage levels coupled by transformer interconnection (the 110 kV HV bus, considered as the slack node; the 20 kV MV grid and the 0.4 kV LV grid level). Wind power plants and industrial loads are connected to the MV buses, whereas, the PV installations and household loads are aggregated for simplicity and connected at the LV grid level. Figure 8 displays the examined grid topology.

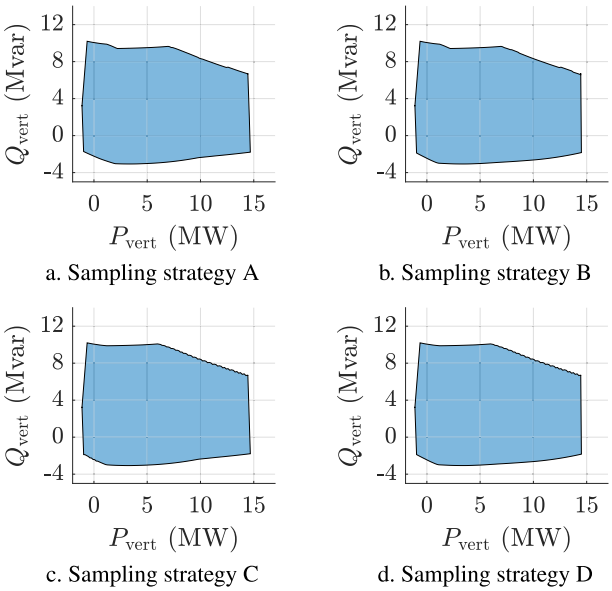

FIGURE 9. Linearized FOR determination with different sampling strategies.

V. RESULTS: AGGREGATION OF DISTRIBUTION GRID POTENTIALS IN THE FORM OF AN FOR

A. COMPARATIVE ASSESSMENT OF FOR DETERMINATION BASED ON LINEARIZED OPTIMIZATION

The linear programming based FOR determination is investigated in this section and the results are segregated based on the applied sampling strategies. Figure 9 presents the corresponding results. The adapted sampling strategies are specified as follows:

- Strategy A: set-point based sampling
- Strategy B: set-point based iterative sampling
- Strategy C: Q_{vert} deviation-reduced sampling
- Strategy D: upper edge simulated using strategy C and strategy B is applied for determination of the lower edge

The increased number of samples ($k = 100$) yield a smoother simulation of edges compared to ($k = 10$) in Figure 1, which is used for demonstration of the algorithm. Comparative observations reveal that Strategy A determines the minimum area, as evident from the upper and lower edges. This is improved upon by Strategy B, which produces an increased area, as evidenced from an accurately sampled lower edge. Strategy C, based on reduced deviations, determines an improved upper edge, however, the lower edge is comparable to that of A. Strategy D determines both edges accurately and presents the maximum observed area of the FOR. Therefore, Strategy D is used for subsequent comparisons with results from other optimization methods. A comparative illustration is presented in Figure 10, validating the observations of area determination. The computation times are tabulated for the discussed strategies. It is observed that the reduced deviations based Strategy C requires the minimum computation time. This is attributed to the increased accuracy of linear sensitivities in approximating the power flow conditions, resulting in decreased successive iterations. In contrast,

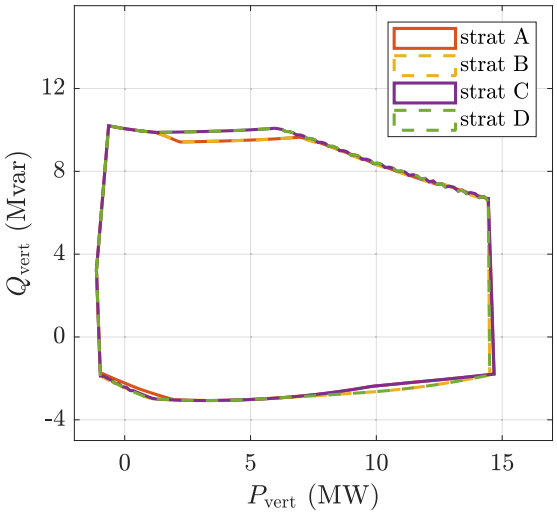

FIGURE 10. Comparison of FOR determined by linear optimization based sampling strategies.

TABLE 1. Computation times of sLP based FOR determination strategies.

	Strategy A	Strategy B	Strategy C	Strategy D
Computation times (s)	5.31	10.34	4.4	9.14

in Strategy B, increased iterations at each sampled boundary point contribute to the highest documented computation time. Strategy D offers a trade-off, by securing an increase in area at the cost of a higher computation time.

B. VALIDATION OF FOR DETERMINED BY SUCCESSIVE LINEAR PROGRAMMING (sLP) WITH ESTABLISHED FOR DETERMINATION ALGORITHMS

Subsequently, comparative investigation of FOR determination with established algorithms, as previously mentioned are displayed in Figure 11. The GAMS, PSO and QCLP based FOR determination results are adopted for comparison from [14], where detailed information of the methods are presented. The comparisons consider the area of the FOR, thus, revealing information on the determined flexibility potential and computation times of the corresponding methods. The GAMS and PSO based methods present improved determinations of the flexibility area compared to the QCLP and sLP. However, the deviations of the edges as evident from the examinations, are not significant. Therefore, comparability and competitiveness of the sLP based method is established.

The corresponding computation times from [14] are tabulated for the different methods and juxtaposed with the computation time required for the sLP. It is noted that the linear programming based FOR presents accurate and comparable representation of the area, at significantly reduced computation times (by a factor of 11 to 70 times). This proves the practicability of usage in real time flexibility assessments.

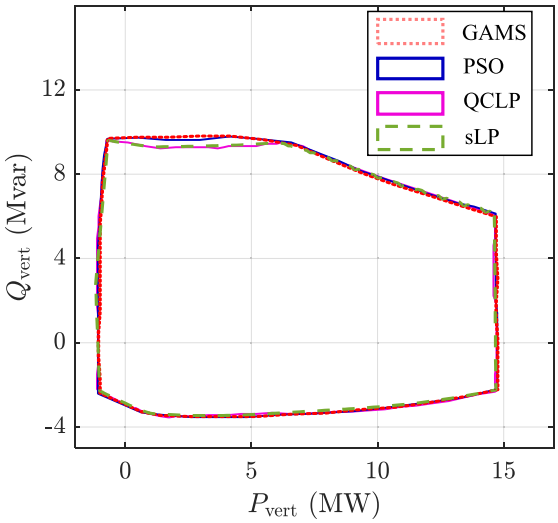

FIGURE 11. FOR comparison with different optimizations methods based on - GAMS, PSO, QCLP and sLP.

TABLE 2. Comparison of computation times.

	GAMS	Modified PSO	QCLP	sLP
Computation times (s)	105	640	164	9.14

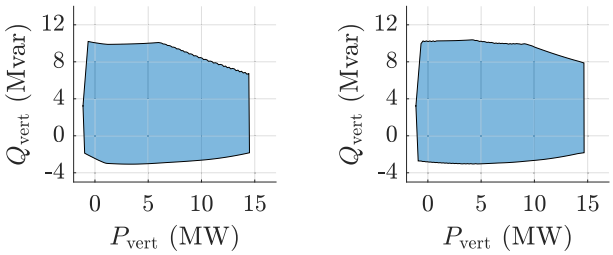

a. FOR without transformer flexibilities

b. FOR with transformer flexibilities

FIGURE 12. Linearized FOR determination with different sampling strategies.

C. ENHANCEMENT OF FOR BY INTEGRATION OF TRANSFORMER TAP-CHANGING FLEXIBILITIES

Integration of transformer tap-changing flexibilities in the linear programming formulation enables an increased FOR area, presented in Figure 12. A comparative assessment with strategies C and D is presented in Figure 13 (the corresponding FOR is depicted by FOR trafo-flex). The increase in area is apparent by comparative observations of the upper edges, whereas, a negligible improvement is noticed for the lower edge. The sampling of the FOR with integrated transformer flexibilities is based on strategy C, as an implementation of strategy D, resulted in inaccuracies and convergence issues. The corresponding computation time is increased to 15.97 s, due to integration of integer (discrete) transformer (OLTC) tap-changing flexibilities.

Table 3 records the area comparisons from Figure 11 and the corresponding computation times which are juxtaposed with the area and computation times of the FOR

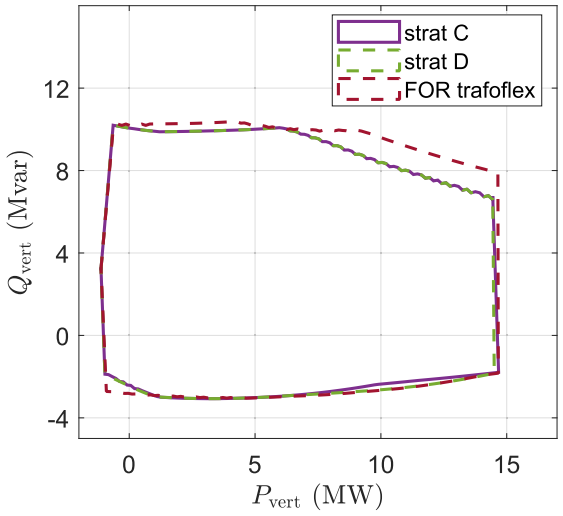

FIGURE 13. Enhancement of FOR by integration of transformer tap-changing flexibilities.

TABLE 3. Comparison of area and computation times.

	Area (% of GAMS FOR)	Computation times (s)
GAMS	1	105
Modified PSO	0.99	640
QCLP	0.985	164
sLP	0.984	9.14
FOR trafoflex	1.046	15.97

enhanced with transformer flexibilities (FOR trafoflex). The results reveal comparability of the sLP based FOR determination, along with area enhancement by integration of transformer flexibilities. Furthermore, fast computation times are observed even after integration of integer transformer tap-set variables.

A comparison of bus voltages and branch power flows are presented in Figure 14. The results are presented for the sampling of upper and lower edges of the FOR. The upper bus voltages correlate with negative reactive power provision at the MV/HV interconnection, whereas, lower bus voltages correspond with positive reactive power provision. A decreasing trend in the bus voltages with increasing sample numbers is observed in both cases, supporting increased voltage drops correlating with increased power flowing from the HV grid level. For the integrated transformer flexibilities, an increase in the lower bus voltages (for samples $k \geq 70$) is attributed to the corrective-iterative actions of the optimizer to prevent voltage limit violations. It is noted that the bus voltages are maintained within permissible limits in both cases (with and without integration of transformer flexibilities).

The power flows are normalized to the maximum branch power transfer capacity. An assessment of normalized branch power flows reveal the adherence to technical constraints.

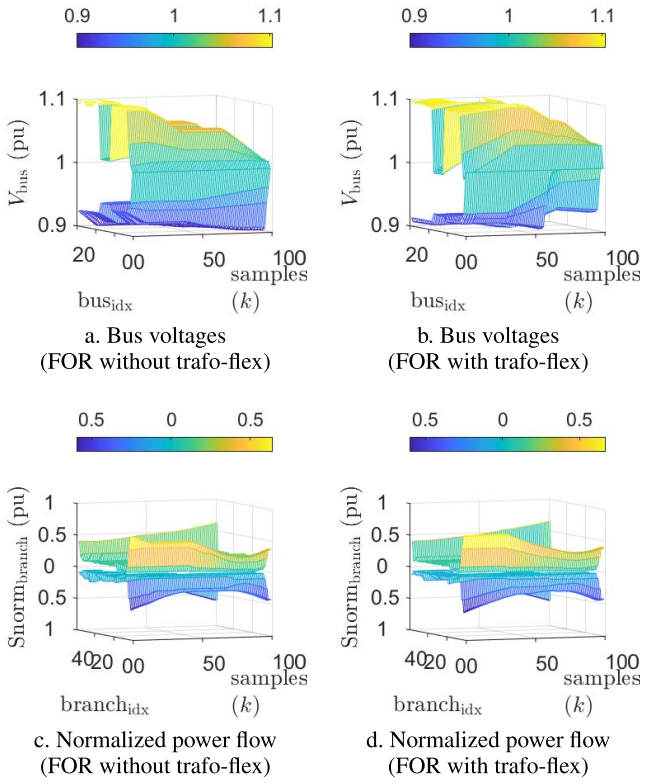

FIGURE 14. Grid state comparison pre- and post-integration of transformer flexibilities.

Since, absolute values are considered, the branch flows for the lower edge determination are plotted against the inverted z-axis. This enables juxtaposition of the sampled power flows for determination of both the upper and lower edges. Furthermore, an increase in MV/HV interconnection power flow is noted ($\text{branch}_{\text{idx}} : 57, 58$) with successive decrement of decentral power injection. This validates the increased power transfer from the HV grid level.

Figure 15 presents a comparison of total reactive power utilization of DERs pre- and post-enhancement of FOR with transformer flexibilities. This is attributed to the additional transformer tap-changer flexibilities that can influence the bus voltages, thereby, influencing the reactive power flow. Increased reactive power transfer through the MV-HV interconnection is enabled, thus, enhancing utilization of the DER reactive power potentials. The increased reactive power utilization corroborates the increased area of FOR, as revealed by Figure 13.

Therefore, in all the above instances, the FOR determined is a 2-dimensional potential PQ-flexibility area at the MV-HV interconnection branch. The results presented are based on step-wise decrement of active power from DERs (since, a MPPT based operation is assumed). Therefore, the resultant flexibility at HV nodes translate to demanded active power and injected/demanded reactive power. The FORs, therefore, reflect the PQ-flexibility at the corresponding HV nodes, and can be used in operational management of the HV grid e.g., voltage control and congestion management.

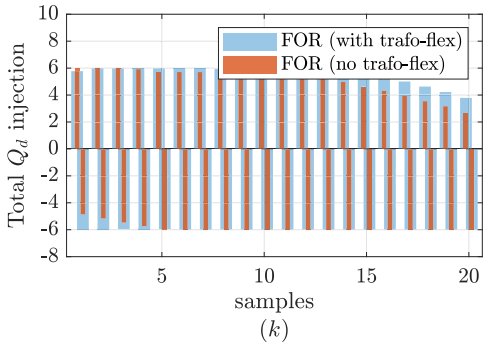

FIGURE 15. Comparison of Q_d utilization pre- and post- integration of transformer flexibilities.

VI. CONCLUSION AND FURTHER WORK

The current research addresses the requirement for increased TSO-DSO cooperation in times of the energy transition. A distribution grid PQ-flexibility aggregation is developed for ancillary service exchanges and operational management planning between the TSO and DSO. The aggregated flexibility area, termed as a feasible operating region (FOR), is determined using successive linear optimization. The results are validated against established methods. Features such as comparability of the results, speed of computation and practicability of usage in real time applications are demonstrated. Enhancement of the flexibility potentials by an increased area of the FOR is achieved by integration of transformer tap-changing flexibilities. The corresponding formulation is developed in a successive mixed integer linear programming environment. Subsequent usage of the FORs in the HV grid operational management or an equivalent flexibility assessment at the HV-EHV interconnections are subjects of further research. Therefore, the investigation presents the groundwork for further studies in multi-voltage level ancillary services exchange and operational management planning.

A constant evolution of further developments in this field of research is foreseen. An integration of cost-prioritization of device flexibilities requires consideration, thus, enabling a corresponding disaggregation to the individual devices in the form of concentric gradients. Research regarding grid uncertainties is undergoing rapid evolution. Moreover, the investigated FOR is determined for radial grids with a single interconnection between the lower and higher voltage levels. This requires further expansion, by development of the FOR over multiple interconnections and consideration of meshed topologies, typical of HV grid levels.

REFERENCES

[1] M. R. Lotz, N. Majumdar, V. Beutel, J. Gerlach, C. Wegkamp, M. Hoffmann, L. Kahl, J. Wussow, H. Schlachter, C. Agert, and M. H. Breitner, "Potentials and technical requirements for the provision of ancillary services in future power systems with distributed energy resources," in *Proc. Conf. Sustain. Energy Supply Energy Storage Syst.*, 2021, pp. 1–8.

[2] S. Lohmann, "The modernisation of distribution grids as a regulatory challenge in Germany," Division Energy Policy-Grids, Federal Ministry Econ. Affairs Energy, Berlin, Germany, Tech. Rep., 2016.

[3] *General Guidelines for Reinforcing the Cooperation Between TSOs and DSOs*, ENTSO-E, Brussels, Belgium, 2021.

[4] *Towards Smarter Grids: Developing TSO and DSO Roles and Interactions for the Benefit of Consumers*, ENTSO-E, Brussels, Belgium, 2021.

[5] *Technical Rules for Operation and Planning by Network Operators—Part 1: Interface Between Transmission and Distribution Systems*, F. VDE, De Witt County, IL, USA, 2017.

[6] M. Heleno, R. Soares, J. Sumaili, R. J. Bessa, L. Seca, and M. A. Matos, "Estimation of the flexibility range in the transmission-distribution boundary," in *Proc. IEEE Eindhoven PowerTech*, Jun. 2015, pp. 1–6.

[7] L. Ageeva, M. Majidi, and D. Pozo, "Analysis of feasibility region of active distribution networks," in *Proc. Int. Youth Conf. Radio Electron., Electr. Power Eng. (REEPE)*, Mar. 2019, pp. 1–5.

[8] D. Mayorga Gonzalez, J. Hachenberger, J. Hinker, F. Rewald, U. Hager, C. Rehtanz, and J. Myrzik, "Determination of the time-dependent flexibility of active distribution networks to control their TSO-DSO interconnection power flow," in *Proc. Power Syst. Comput. Conf. (PSCC)*, Jun. 2018, pp. 1–8.

[9] S. Riaz and P. Mancarella, "On feasibility and flexibility operating regions of virtual power plants and TSO/DSO interfaces," in *Proc. IEEE Milan PowerTech*, Jun. 2019, pp. 1–6.

[10] J. Silva, J. Sumaili, R. J. Bessa, L. Seca, M. A. Matos, V. Miranda, M. Caujolle, B. Goncer, and M. Sebastian-Viana, "Estimating the active and reactive power flexibility area at the TSO-DSO interface," *IEEE Trans. Power Syst.*, vol. 33, no. 5, pp. 4741–4750, Sep. 2018.

[11] M. Rossi, G. Viganò, D. Moneta, M. T. Vespucci, and P. Pisciella, "Fast estimation of equivalent capability for active distribution networks," *CIRED-Open Access Proc. J.*, vol. 2017, no. 1, pp. 1763–1767, Oct. 2017.

[12] D. A. Contreras and K. Rudion, "Improved assessment of the flexibility range of distribution grids using linear optimization," in *Proc. Power Syst. Comput. Conf. (PSCC)*, Jun. 2018, pp. 1–7.

[13] D. A. Contreras and K. Rudion, "Impact of grid topology and tap position changes on the flexibility provision from distribution grids," in *Proc. IEEE PES Innov. Smart Grid Technol. Eur. (ISGT-Europe)*, Sep. 2019, pp. 1–5.

[14] M. Sarstedt, L. Kluß, J. Gerster, T. Meldau, and L. Hofmann, "Survey and comparison of optimization-based aggregation methods for the determination of the flexibility potentials at vertical system interconnections," *Energies*, vol. 14, no. 3, p. 687, Jan. 2021.

[15] M. Kalantar-Neyestanaki, F. Sossan, M. Bozorg, and R. Cherkaoui, "Characterizing the reserve provision capability area of active distribution networks: A linear robust optimization method," *IEEE Trans. Smart Grid*, vol. 11, no. 3, pp. 2464–2475, May 2020.

[16] S. Wang and W. Wu, "Stochastic flexibility evaluation for virtual power plant by aggregating distributed energy resources," 2020, *arXiv:2006.16170*.

[17] Z. Tan, H. Zhong, Q. Xia, C. Kang, X. S. Wang, and H. Tang, "Estimating the robust P-Q capability of a technical virtual power plant under uncertainties," *IEEE Trans. Power Syst.*, vol. 35, no. 6, pp. 4285–4296, Nov. 2020.

[18] D. A. Contreras and K. Rudion, "Time-based aggregation of flexibility at the TSO-DSO interconnection point," in *Proc. IEEE Power Energy Soc. Gen. Meeting (PESGM)*, Aug. 2019, pp. 1–5.

[19] S. Müller, D. A. Contreras, H. Früh, K. Rudion, C. Exner, and A. von Haken, "Online aggregation of the flexibility potential in distribution grids using state estimation," Tech. Rep., 2021.

[20] D. A. Contreras, S. Müller, and K. Rudion, "Congestion management using aggregated flexibility at the TSO-DSO interface," in *Proc. IEEE Madrid PowerTech*, Jun. 2021, pp. 1–6.

[21] M. Sarstedt and L. Hofmann, "Monetarization of the feasible operation region of active distribution grids based on a cost-optimal flexibility disaggregation," *IEEE Access*, vol. 10, pp. 5402–5415, 2022.

[22] M. Knittel, J. Massmann, A. Schnettler, and D. Kamenschikow, "Future operational concepts for reactive power compensators in transmission grids," in *Proc. Medit. Conf. Power Gener., Transmiss., Distrib. Energy Convers. (MEDPOWER)*, 2018, pp. 1–5.

[23] M. Knittel, N. Majumdar, M. Schneider, N. Thie, and A. Moser, "Voltage control in transmission grids considering uncertainties of renewable energy sources," in *Proc. 6th IEEE Int. Energy Conf. (ENERGYCon)*, Sep. 2020, pp. 580–585.

[24] N. Majumdar, M. Sarstedt, T. Leveringhaus, and L. Hofmann, "Linearized optimization for reactive power dispatch at transmission grid level considering discrete transformer tap-settings," in *Proc. 13th IEEE PES Asia Pacific Power Energy Eng. Conf. (APPEEC)*, Nov. 2021, pp. 1–6.

[25] A. T. Saric and A. M. Stankovic, "A robust algorithm for Volt/Var control," in *Proc. IEEE/PES Power Syst. Conf. Expo.*, Mar. 2009, pp. 1–8.
[26] M. Sarstedt, T. Leveringhaus, L. Kluß, and L. Hofmann, "Comparison of convexificated SQCQP and PSO for the optimal transmission system operation based on incremental in-phase and quadrature voltage controlled transformers," in *Proc. Conf. Sustain. Energy Supply Energy Storage Syst.*, 2021, pp. 1–8.
[27] T. Leveringhaus and L. Hofmann, "Comparison of methods for state prediction: Power flow decomposition (PFD), AC power transfer distribution factors (AC-PTDFs), and power transfer distribution factors (PTDFs)," in *Proc. IEEE PES Asia–Pacific Power Energy Eng. Conf. (APPEEC)*, Dec. 2014, pp. 1–6.
[28] T. Leveringhaus and L. Hofmann, "Combined and optimized redispatch management of multiple congestions and voltage deviations with active and reactive power based on AC-PTDFs with distributed slack," in *Proc. IEEE Power Energy Soc. Gen. Meeting*, Jul. 2015, pp. 1–5.
[29] *Reactive Power Capability and Interconnection Requirements for PV and Wind Plants*, E.-E. S. I. Group, New Delhi, India, 2021.
[30] O. L. Mangasarian, "Absolute value equation solution via linear programming," *J. Optim. Theory Appl.*, vol. 161, no. 3, pp. 870–876, Jun. 2014.
[31] *MATLAB Optimization ToolBox*, MathWorks, Natick, MA, USA, 2019.
[32] M. Sarstedt, N. Majumdar, C. Blaufuß, and L. Hofmann, "Dataset: Multi-voltage-level electric power system data sets-survey and comparison of optimization-based aggregation methods for the determination of the flexibility potentials at vertical system interconnections," Tech. Rep., 2020, doi: 10.25835/0013459.

NEELOTPAL MAJUMDAR was born in Kolkata, West Bengal, India, in 1993. He received the B.Tech. degree in electrical engineering from the Maulana Abul Kalam Azad University of Technology (formerly West Bengal University of Technology), in 2016, and the M.Sc. degree in electrical power engineering from the RWTH Aachen University, Aachen, Germany, in 2020. He is currently pursuing the Ph.D. degree in electrical engineering with the Institute of Electric Power Systems, Leibniz Universität Hannover. His research interests include optimized ancillary services provision between multiple voltage levels and optimal operation under consideration of uncertainties.

MARCEL SARSTEDT was born in Hanover, Lower Saxony, Germany, in 1992. He received the B.Sc. and M.Sc. degrees in power engineering from the Leibniz Universität Hannover, Hannover, in 2017. He is currently pursuing the Ph.D. degree in electrical engineering with the Institute of Electric Power Systems, Leibniz Universität Hannover. His research interests include grid control concepts, ancillary services, and TSO/DSO-cooperation.

LEONARD KLUß was born in Hannover, Germany, in 1990. He received the B.S. and M.S. degrees in power engineering from Leibniz University, Hannover, in 2015 and 2018, respectively, where he is currently pursuing the Ph.D. degree in electrical engineering with the Institute of Electrical Power Systems. His research interests include linear and non-linear optimization and the optimization under uncertainties in the field of power engineering.

LUTZ HOFMANN was born in Bad Oeynhausen, Lower Saxony, Germany, in 1968. He received the Dipl.-Ing. and Dr.-Ing. degrees from the Leibniz Universität Hannover, Hanover, Germany, in 1994 and 1997, respectively. In 2002, he concluded his professorial dissertation in electric power engineering. In 2002 and 2003, he was a Project Manager at the engineering and consultant company Fichtner, Stuttgart, Germany. From 2004 to 2007, he was a German Transmission System Operator at the Network Planning Department, E.ON Netz GmbH, Bayreuth, Germany. Since 2007, he has been a Full Professor and the Head of the Institute of Electric Power Systems, Leibniz Universität Hannover. Since 2011, he has also been the Head of the Department of Transmission Grids, Fraunhofer IWES, Kassel, Germany. His current research interests include modeling and simulation of electric power systems, integration of renewable and decentralized energy sources, and power quality.